Programmable DNA shell scaffolds for directional membrane budding

Michael T. Pinner[1,2] and Hendrik Dietz[1,2]

[1] Laboratory for Biomolecular Nanotechnology, Department of Biosciences, School of Natural Sciences, Technical University of Munich, Am Coulombwall 4a, 85748 Garching, Germany.

[2] Munich Institute of Biomedical Engineering, Technical University of Munich, Boltzmannstraße 11, 85748 Garching, Germany.

Abstract

In the pursuit of understanding and replicating biological processes at the nanoscale, controlling cellular membrane dynamics has emerged as a key area of interest. Here, we report a system capable of controlling directional membrane budding through a mechanism mimicking virus assembly on a lipid membrane. We employed three-dimensional DNA origami techniques to construct icosahedral shells that self-assemble and interact with the lipid membranes of giant vesicles via cholesterol moieties. The membrane-constrained assembly of shells results in the programmable formation of DNA-shell-coated vesicles or vesicle-coated DNA shells, effectively demonstrating membrane curvature induction and spontaneous neck scission. We further show that these processes can be combined into a 2-step budding reaction, giving rise to nested bivesicular objects with DNA shells encapsulated between two lipid vesicles. Our findings replicate key aspects of natural endocytic and exocytic pathways, and open new avenues for the exploration of membrane mechanics and for applications in targeted drug delivery and synthetic biology.

Introduction

Membrane budding is a ubiquitous biological phenomenon in which parent lipid membranes release daughter vesicles for the transport of materials across the membrane. It plays a pivotal role in the lifecycle of many viruses, particularly enveloped viruses, and is intimately tied to virus infection and virus release processes from host cells[1]. Understanding and

potentially controlling budding processes may contribute to comprehending viral pathogenesis and developing antiviral strategies. Further, in clathrin-mediated endocytosis (CME), clathrin, with its distinctive triskelion shape, remodels lipid membranes by binding to membrane-bound receptor-adaptor protein complexes, followed by self-assembly into spherical cage-like structures that induce curvature in the cell membrane[2–4]. This process culminates in the formation of a clathrin-coated vesicle[2]. Artificial membrane budding systems are of particular interest as they allow studying the underlying mechanics in a controlled environment, potentially offering a deeper understanding of cellular processes. Other benefits may include the development of improved drug delivery systems or, in the context of immunology, vaccine vectors by producing non-infectious but immunogenic biopsies of pathogenic cells. They may also support the creation of synthetic cells or organelles, contributing to the field of synthetic biology where there is growing interest in building biological systems with novel functions.

Scaffolded DNA origami is a unique method to self-assemble defined 3D structures on the nanoscale using DNA as a building material[5–7]. A several kilobases long, single-stranded 'scaffold' strand is mixed with an array of shorter oligonucleotides and exposed to a thermal annealing ramp to drive the folding of the DNA origami structure. The programmability of Watson-Crick base pairing interactions has allowed the production of nanostructures ranging from simple bricks[6] to giga-Dalton-sized multimeric assemblies[8–11]. The relative ease of producing DNA origami structures expanded the experimental toolkit on the nanoscale and accelerated research towards synthetic biology applications, including efforts to interact with and manipulate natural membranes.

Previous efforts in the field related to lipid membranes have successfully tethered membrane-spanning DNA nanopores of various complexity to lipid bilayers using hydrophobic moieties such as cholesterol[12], ethyl-phosphorothioate[13] or tetraphenylporphyrin[14]. Notably, cholesterol-labelled DNA origami objects tethered to lipid membranes retain diffusive mobility influenced by factors like linker oligo length[15], paving the way for the 2D assembly of monomeric structures into multimeric lattices[16]. Prior studies have also shown that both curved[17–19] and planar[17] origami structures can induce tubulation in giant unilamellar lipid vesicles (GUVs). On-membrane polymerisation of origami structures into 2D lattices likewise resulted in the deformation of the underlying membrane reminiscent of clathrin networks[16,20–22].

In the biological systems that inspire our work here, membrane curvature changes are often induced by curved proteins, including Clathrin and Bin/amphiphysin/Rvs (BAR) domain proteins. These proteins remodel lipid bilayers through mechanisms like the insertion of hydrophobic residues into one of the leaflets of the bilayer, causing asymmetrical surface area expansion, imprinting the protein's curved shape onto the bilayer through strong binding, and crowding effects[23,24]. Further, BAR domain proteins also act as curvature sensors and recruit the GTPase dynamin to the bud neck, promoting scission[2,25]. Interestingly, the amphipathic helix used by N-BAR proteins for membrane anchoring alone can constrict and sever the bud neck[26]. This mechanism is echoed in biological entities like the influenza virus M2 protein, which facilitates membrane scission through an amphipathic helix independent of its ion channel function or the cellular budding machinery[27].

Building upon this foundational work, we have developed an artificial, DNA origami-based membrane budding system with spontaneous neck scission. At its core are three-dimensional membrane-interacting triangular subunits constructed from DNA with bevelled edges[28]. Strategically placed shape-complementary protrusions and recesses at the triangles-edges direct the self-assembly of these triangular subunits into icosahedral shells through adhesive base pair stacking interactions[29]. Interactions with lipid membranes of giant vesicles (GVs) were promoted using cholesterol moieties placed on specific triangular surfaces. We hypothesised that membrane deformation processes may be sufficient for the spontaneous scission of the bud neck without the need for active constriction by GTPases like dynamin[25]. Indeed, the self-assembly of membrane-bound triangles induced local curvature and finally led to the formation and eventual scission of buds. The positioning of cholesterol determined whether the bud-formation occurs inward or outward from the source vesicle, leading to DNA-shell-coated vesicles (DCV) and vesicle-coated DNA shells (VCD), respectively.

Results

1. DNA-Shell-Coated Vesicles

We adapted a previously developed programmable icosahedral shell canvas, in which twenty equilateral DNA origami triangles form a closed icosahedron triggered by elevated concentrations of magnesium chloride for membrane-supported assembly[28]. To provide the necessary hydrophobic interactions required for association with lipid membranes, we incorporated multiple cholesterol-bearing oligonucleotides at the shell-inward-facing surface of the constituent triangular DNA origami subunits (Fig. 1a & Supplementary Fig. 1). We

101 hypothesised that the 2D diffusion of triangles on a fluid membrane can support the assembly
102 of icosahedral shells whilst pulling membrane material along, resulting in increasingly
103 deformed membrane buds growing away from the parent membrane until the bud neck is cut
104 and a DNA-shell-coated vesicle (DCV) is released into solution.
105
106 We screened cholesterol density and positioning to balance the solubility of the triangles with
107 membrane affinity (Supplementary Fig. 2a) and then validated the assembly of cholesterol-
108 modified triangles into the expected icosahedral shells in the absence of membranes.
109 Introducing cholesterol moieties resulted in a shift from the previously observed relatively
110 uniform icosahedral shells to a mixture containing both octahedral and icosahedral shells.
111 This variation was controllable: by limiting the reach of each cholesterol moiety, as shown in
112 Supplementary Figure 2b, we could largely revert the assembly to predominantly icosahedral
113 structures. The addition of lipid membranes into the system introduced another variable,
114 again leading to the occurrence of octahedral structures. This tendency varied depending on
115 the amount of cholesterol per triangle, detailed in Supplementary Figures 3 and 4. We believe
116 this effect arises from a complex interplay of forces, including the attraction between
117 cholesterols and membranes, membrane deformation, and elastic deformation within the
118 shells caused by less-than-ideal angles between the triangle subunits. Nevertheless,
119 octahedral and icosahedral forms were both considered suitable for our objectives.
120
121 We chose giant vesicles (GVs) composed of 1,2-dioleoyl-sn-glycero-3-phosphocholine
122 (DOPC) with up to 1% of fluorescently labelled 1,2-dioleoyl-sn-glycero-3-
123 phosphoethanolamine (DOPE) as model membranes to study membrane deformation and
124 budding. Vesicles were grown by gentle swelling of dried lipid cakes on polyvinyl alcohol
125 (PVA) coated surfaces[30] in folding buffer containing 5 mM $MgCl_2$ and 300 mM NaCl or 320
126 mM CsCl. Triangles bearing linker handles were hybridised to chol-bearing antihandles at a
127 1.5-fold excess for at least 30 min at room temperature. Thereafter, aliquots of GVs and chol-
128 decorated triangles were mixed to anchor the nanostructures to the vesicles. GVs could be
129 readily coated with the thus-modified DNA triangle subunits (Fig. 1b). Non-specific binding
130 of triangle subunits to vesicles was suppressed by including NaCl in the reaction mixture,
131 ensuring triangles bind vesicles in the designed orientation as defined by the location of their
132 cholesterol moieties[19].
133
134 We triggered DNA shell assembly on membranes by increasing the $MgCl_2$ concentration and
135 incubating the solution at 37 °C for up to multiple days. Imaging the samples by negative

136 stain transmission electron microscopy (TEM) revealed DCVs appearing as dark DNA shells
137 that fully engulfed lipid vesicles appearing as bright rings in the images (Fig. 1c, top right).
138 Occasionally, the shell-enclosed vesicles appeared deformed or cracked, which we attribute
139 to staining and drying artefacts. To study DCVs in their native conditions, we also acquired
140 micrographs of vitrified samples by cryogenic transmission electron microscopy (cryoEM, Fig.
141 1c, bottom right). The data generally agrees with the conclusions drawn from negative stain
142 TEM data, but the enclosed vesicles seen by cryoEM rarely did have any defects except for
143 occasionally encapsulating even smaller vesicles themselves. In the cryo-EM micrographs,
144 the vesicle typically fills up the available space inside the origami shell, with the membrane
145 in direct contact with the enclosed DNA shell. These findings support budding triggered by
146 shell assembly on a parent membrane as the predominant mechanism of DCV formation as
147 opposed to capturing small unilamellar vesicles (SUVs). We also note that variants of the
148 triangle subunits that cannot form shells also did not produce DCVs, supporting the idea that
149 shell assembly on membranes is an essential driver for DCV formation (Supplementary Fig.
150 5).
151
152 As our setup involves budding off nanoscopic vesicles that are multiple orders of magnitude
153 smaller than their parent vesicles, direct observation of DCV formation from GVs is
154 challenging. However, when using large vesicles (LVs), direct observation of intermediate
155 steps in DCV formation is possible using cryoEM. To this end, we thoroughly washed GVs to
156 remove contaminating SUVs and then pushed them through a 200 nm pore filter to produce
157 LVs of roughly that size. Furthermore, we shortened the on-membrane incubation of origami
158 triangles to capture growing buds before they are released into the solution as DCVs. We
159 mixed vesicles with isosmotic $MgCl_2$ solutions to avoid artefacts by vesicle deflation. We thus
160 succeeded in acquiring micrographs that show various intermediate states of deformation of
161 the parent vesicle induced by the emerging DNA shells (Fig. 2a). Whilst membrane patches
162 free of DNA triangle subunits appear undisturbed, those with triangle objects on them had
163 deformations that matched the curvature of the triangle assemblies. Notably, some vesicles
164 have multiple buds with a clearly visible bud neck. This image data further supports the notion
165 that budding is the mechanism behind DCV formation from LVs and GVs. Occasionally, we
166 also found DCVs where the DNA origami shell had assembly “scars” consisting of one or two
167 missing triangles (Fig. 2b). We believe these scars to be another signature of budding,
168 considering that the increasingly high curvature at the bud neck can become a steric barrier
169 to completion of the DNA origami shell. In this scenario, spontaneous membrane scission

170 competes with the completion of the DNA origami shell, which may occasionally lead to such
171 assembly scars.
172
173 To evaluate whether the lipid vesicles were fully enclosed by well-ordered icosahedral or
174 octahedral DNA shells, we recorded single-axis tilt series to generate tomograms, allowing
175 us to study DCVs in 3D (Fig. 2c). The representative tomograms confirm full engulfment of
176 the vesicle by closed shells featuring the symmetry properties expected by design.
177
178 We next studied the influence of osmolality on DCV formation. The addition of concentrated
179 magnesium chloride solution as a trigger for icosahedral shell assembly inevitably increases
180 the osmolality of the sample buffer and may thus alter the biophysical properties of the
181 membrane by deflation of GVs. Indeed, hyperosmotic stress has previously been exploited
182 to alter vesicle shape by membrane-bound DNA origami[19]. We tested the influence of
183 osmolality in DCV formation by triggering DNA shell assembly using either hyperosmotic or
184 isosmotic $MgCl_2$ solutions (Fig. 2d). We measured the extent of DCV formation by agarose
185 gel electrophoresis using fluorescent labels on DNA origami components and a fraction of
186 the lipids constituting the GVs (Supplementary Fig. 6). Fluorescent lipid bands colocalised
187 only with the higher-order shell assemblies and were virtually absent at the level of
188 monomeric triangles. Direct comparison of DCVs formed under hyperosmotic and isosmotic
189 conditions reveals that osmotic pressure differences do not noticeably influence assembly
190 yields as measured by comparing the brightness of lipid bands relative to the DNA shell band
191 in the gels. Hyperosmotic deflation of GVs, therefore, is not required for DCVs to form.
192
193 In our study, we primarily used vesicles made of 99.0 – 99.5% DOPC, supplemented with a
194 small fraction of fluorescently labelled DOPE species. Our initial theory suggested that
195 introducing cholesterol into the outer layer of the vesicle membrane via DNA triangle tethering
196 might be crucial for DCV formation. To evaluate this, we introduced 3% biotinylated DOPE
197 into the lipid mixture and prepared GVs from it. Instead of attaching cholesterol-modified
198 oligonucleotides to the origami triangles, we used biotinylated oligonucleotides connected to
199 NeutrAvidin (b-NAv). NeutrAvidin's unoccupied binding sites could then capture the vesicles'
200 biotinylated lipid components, allowing the DNA triangles to attach to the membrane without
201 directly inserting cholesterol or other foreign anchors into the membrane leaflets. Interestingly,
202 we observed the formation of OCVs under both hyperosmotic and isosmotic conditions using
203 this approach, as shown in Figure 2e. Furthermore, excess cholesterol-modified
204 oligonucleotides with a different sequence did not influence this result. This indicates that the

205 integration of cholesterol into the membrane is not necessary for the formation of DCVs and
206 supports the notion that DCVs are driven by curvature that emerges from the assembly of
207 the DNA origami shells.
208
209 We also investigated the efficiency of DCV assembly as a function of the average parent
210 vesicle size. To this end, we passed GVs through filters with 400, 200, or 50 nm pores,
211 producing vesicles of specific sizes. We then used these vesicles in a controlled lipid-to-DNA
212 triangles stoichiometry budding assay to examine the efficiency of DCV formation, which we
213 measured by quantifying DNA and lipid band intensities of DCVs ran on an agarose gel. As
214 Figure 2f shows, there is a defined optimal lipid quantity for each vesicle size except for GVs.
215 Interestingly, whereas DCV yield curves for SUVs and LVs were quite similar, the curve for
216 GVs peaked and then plateaued over a broad lipid quantity range (see Figure 2g). To test
217 whether triangles also assemble in solution into partial shells (i.e. half icosahedra) and then
218 subsequently form a bud on GVs, we inverted the DCV preparation protocol, i.e. we first
219 preassembled shells in the absence of membranes and then added GV with a temporal offset
220 of several hours, which led to a substantial decrease in DCV yield (Supplementary Fig. 7).
221 This data further supports the notion that on-membrane assembly of shells is a key driver for
222 bud formation.
223
224 The DCVs prepared thus far formed in a process reminiscent of exocytosis, where vesicles
225 bud outwardly from a cell, but with the difference that the components forming the bud are
226 approaching from the exterior of the parent vesicle. We were also able to invert the
227 directionality toward mimicking endocytic processes. To this end, we placed the cholesterol
228 moieties that promote membrane association on the shell-outward face of the triangle
229 subunits. Shell assembly on the membrane should then lead to the formation and release of
230 a vesicle-coated DNA shell (VCD) into the lumen of the parent vesicle (Fig. 3a), effectively
231 creating an organelle- or endosome-like compartment. We extruded GVs through 200 nm-
232 sized pore filters and prepared triangles carrying one cholesterol moiety per side. Direct
233 imaging with cryoEM (Fig. 3b) revealed VCDs, i.e. lipid vesicles tightly wrapped around
234 icosahedral shells located within their parent vesicles. Occasionally, we also observed free
235 VCDs presumably set free by the bursting of the parent vesicle. As with DCVs, we
236 occasionally spotted scars on the VCDs where the DNA shell was visibly missing triangles.
237
238 Finally, we tested if bivesicular shell structures could be produced by combining both
239 outward and inward budding in a two-step process using triangle subunits with sequence-

240 orthogonal linker handles on their top and bottom faces (Fig. 3c). First, we hybridised
241 cholesterol-modified DNA strands to the linker handles on the bottom face of the triangles
242 and mixed the DNA triangles with GVs to produce DCVs as described earlier. We then
243 centrifuged the sample at low speed to remove some of the remaining GVs, followed by
244 ultracentrifugation of the supernatant to pellet any remaining vesicles, DNA components and
245 DCVs. Most of the supernatant was discarded, and the pellet was resuspended in the
246 remaining volume. We then prepared LVs by extruding GVs through 200 nm pore size filters
247 and added cholesterol-modified oligonucleotides to this vesicle mixture to cover the
248 membrane with single-stranded linker handles. The sequence of these strands is
249 complementary to the single-stranded linker handles on the shell-outer face of the triangles
250 but orthogonal to those on the shell-inner face used in the first step for outward budding.
251 Finally, the DCV concentrate was mixed with the LVs covered with complementary linker
252 handles, and the mixture was incubated at 37 °C. We analysed the sample using cryoEM and
253 indeed found vesicle-coated DCVs (VCDCVs). Like VCDs, VCDCVs were typically inside of
254 their respective parent vesicle. These particles may be considered examples of synthetically
255 created organelles featuring a cytoplasm-like compartment (the inner vesicle) and a
256 periplasm-like compartment (the void between the outer envelope membrane and the inner
257 lipid membrane). The DNA icosahedral shell acts as a stabilising mechanical skeleton,
258 offering engineering options for including additional molecular functionalities.

259 Discussion

260 A key difference between our system and cellular clathrin-mediated endocytosis is the
261 absence of active neck scission. In cells, dynamin is needed for vesicle release[31], but in our
262 system, DNA-shell-coated vesicles (DCVs) release spontaneously, albeit after a comparably
263 long incubation time. Neck scission may currently represent the kinetic bottleneck in DCV
264 formation. Different membrane anchors, such as the influenza virus protein M2, could
265 improve the system's kinetics. Previously, cholesterol-labelled DNA objects of varying
266 shapes have been described to cause vesicle tubulation, a phenomenon also observed with
267 Clathrin's adaptor protein epsin[17–19,32]. We find that the DNA origami's membrane anchor type
268 does not significantly affect bud formation. The assembly of DNA triangles into shells is the
269 primary driver of bud formation, as these shells imprint their curvature onto the membrane,
270 shaping the buds. We also found that DCV formation varies with vesicle size and lipid quantity,
271 where high lipid quantities contained in GV reservoirs yielded good amounts of DCVs,
272 whereas budding from smaller vesicles had reduced yields.
273

We could trigger inward budding by shifting the position of cholesterols from the inner face to the outer face of a triangle. When using DCVs instead of monomeric triangles, we could produce nested bivesicular structures carrying both an inner and an outer vesicle, demonstrating the system's modularity and level of control. However, further optimisation is needed to improve yields and reduce aggregation for efficient production of bivesicular DNA shells.

In conclusion, our DNA origami-based system offers an attractive approach to engineer vesicles of controlled size featuring addressable endo- or exoskeletons. By performing the budding on GVs containing molecules of interest, the budding system could be further developed toward molecular payload applications. Using nested bivesicular structures, it becomes possible to design scenarios where two different molecular payloads are delivered simultaneously but separately. This work may thus pave the way for innovative applications in targeted drug delivery, vaccine development, and synthetic biology. Future explorations could extend to fine-tuning the system's efficiency and exploring the breadth of its applications, particularly in medical and biotechnological fields. The potential to manipulate membrane dynamics at the nanoscale also opens new horizons in synthesising artificial cells and organelles, offering a valuable tool for researchers in their quest to harness the power of nanotechnology for practical and therapeutic purposes.

Acknowledgements

The authors acknowledge financial support received from the European Research Council Advanced Grant awarded to H.D. (grant agreement 101018465) and the Deutsche Forschungsgemeinschaft for the Gottfried Wilhelm Leibniz Program grants provided to H.D. This project has received funding from the European Union’s Horizon 2020 research and innovation programme under the Marie Skłodowska-Curie grant agreement No 765703. We thank Andreas Bausch for technical assistance, Björn Högberg for discussions and Volodymyr Mykhailiuk for help with illustrations.

Author contributions

The research was performed by M.P., supervised by H.D. The manuscript was written by M.P. and H.D.

Figures & Captions

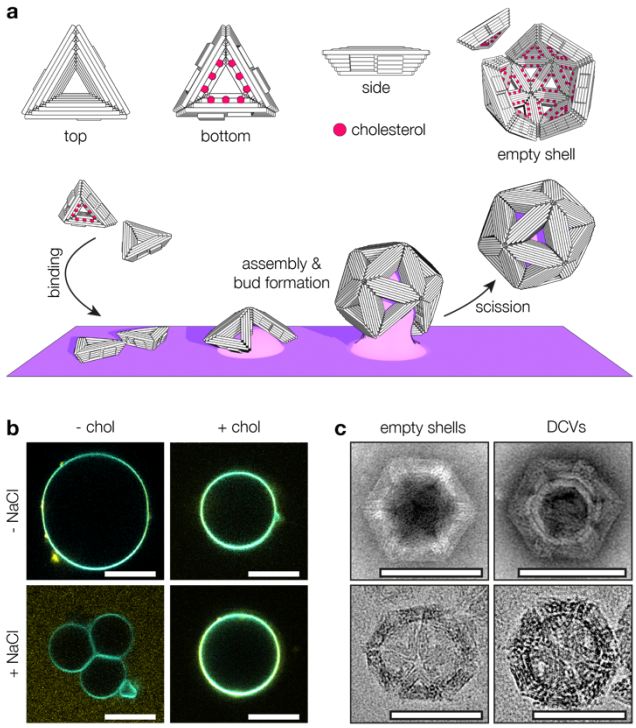

Figure 1: DNA-shell-coated vesicle formation

a, Schematic of a DNA origami triangle-based membrane budding system. The triangular structures are decorated with cholesterol moieties to tether them to the membrane of a lipid vesicle. Upon increasing the $MgCl_2$ concentration, the triangles self-assemble into DNA shells, pulling the membrane underneath along to form a bud. Eventually, the bud neck is cut, and a DNA-shell-coated vesicle (DCV) is released. **b,** Attachment of DNA origami triangles (yellow) onto giant vesicles (GVs, cyan). Triangles will adsorb onto GVs even if they are not decorated with cholesterol (top left & right panel). However, adding sodium chloride suppresses this non-specific adsorption (bottom left panel), and membrane binding will only occur if cholesterol is attached to the triangle (bottom right panel). Scale bars: 50 µm. **c,** Transmission electron micrographs of empty DNA shells and DCVs. In negative-stain TEM (top panels), lipid vesicles within DCVs appear as white rings inside the DNA shell. In cryogenic electron microscopy (cryoEM, bottom panels), the vesicle is visible as a dark ring inside the DNA shell. Scale bars: 100 nm.

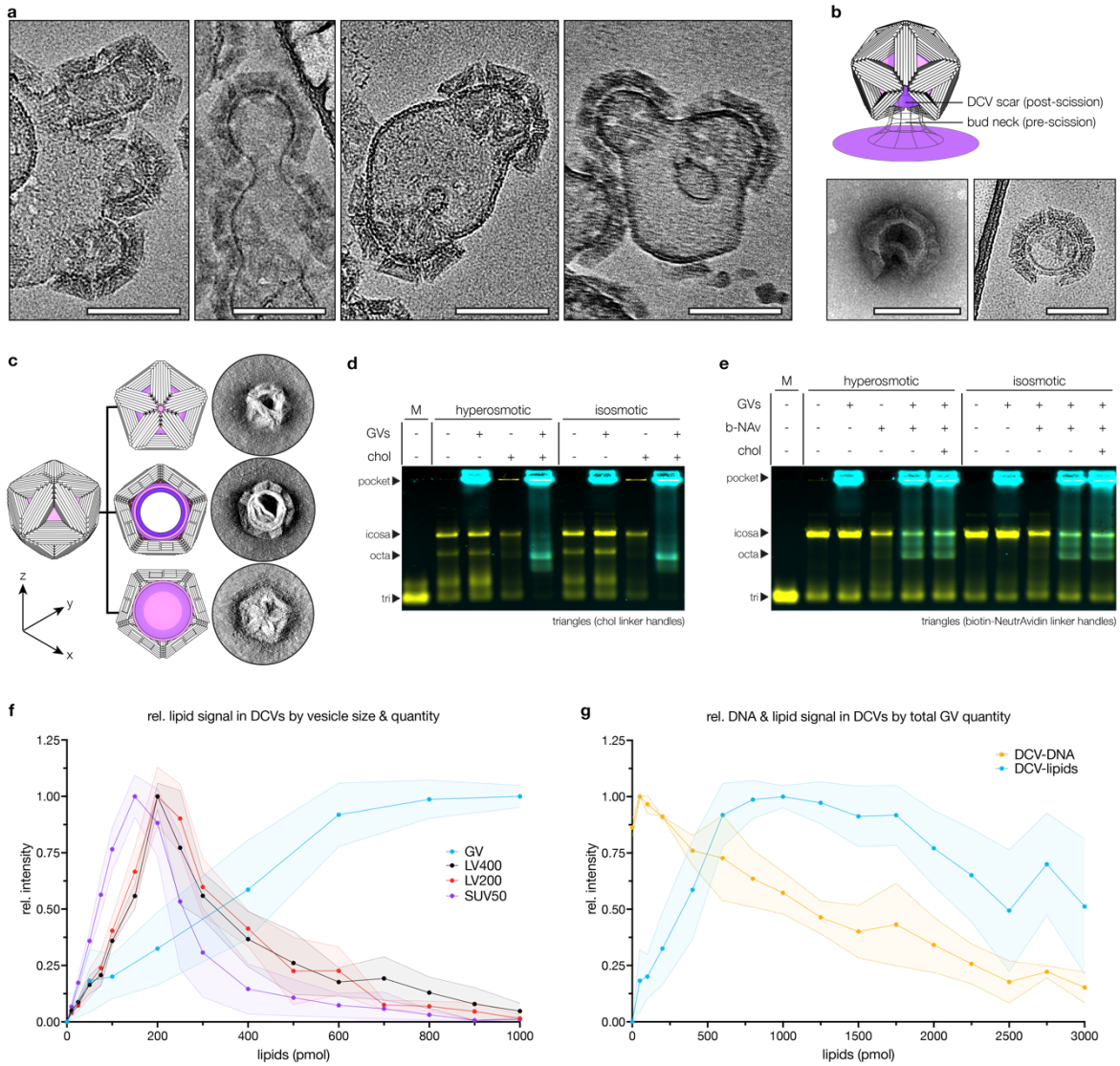

Figure 2: DNA-shell-coated vesicles form by membrane budding.

a, CryoEM micrographs of large vesicle (LV) deformation upon assembly of membrane-bound DNA origami triangles. Bud curvature closely follows the intrinsic curvature of the assembling. Scale bars: 100 nm. **b,** DCVs occasionally appear incomplete with visible 'scars' of missing triangles. The bud neck prevents closure of the DNA shell by steric hindrance, resulting in a gap in the origami shell that remains visible after scission of the neck. Left panel: negative-stain TEM; Right panel: cryoEM. Scale bars: 100 nm. **c,** Tomogram of an icosahedral DCV depicted as summed up z-slices of the top, central and bottom segments of the DCV. The topmost segment appears as a tilted, incomplete pentamer. The central segment reveals a lipid vesicle trapped within the origami shell. The bottommost segment is a pentameric shell cap. **d,** Agarose gel of DCVs prepared under hyperosmotic and isosmotic conditions. Lipid material (cyan, DOPE-Atto488) remains in the pockets unless cholesterol-hybridised triangles (yellow, Atto643) are mixed with GVs. Lipids form bands colocalising with octahedral and

340 icosahedral shells but not with monomeric triangles. Thus, lipid material is dragged into the
341 gel as DCVs. Gel pockets were oversaturated for better band visualisation. **e,** Agarose gel of
342 DCVs prepared by using biotin-NeutrAvidin interactions to connect origami triangles (yellow,
343 Atto643) and GVs (cyan, DOPE-Atto488) containing a fraction of biotinylated DOPE. **f,**
344 Relative lipid band intensities of DCVs prepared from vesicles of different sizes and quantities.
345 **g,** Relative lipid and DNA band intensities of DCVs obtained from different quantities of GVs.
346

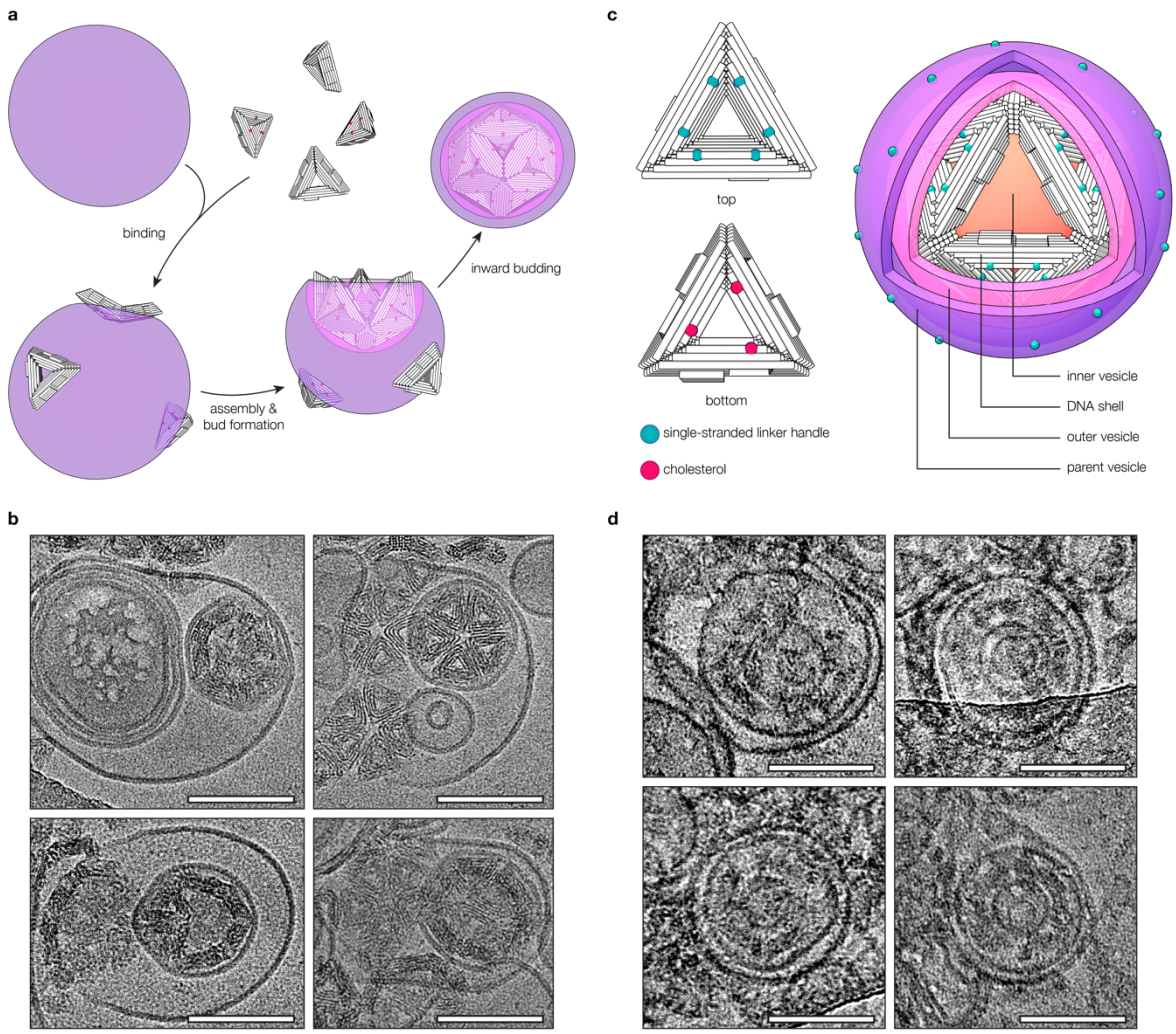

Figure 3: Vesicle-coated DNA shells and multivesicular DNA shells

a, Illustration of vesicle-coated DNA shell (VCD) formation by budding into a parent vesicle. The budding direction is reversed with respect to DCVs by shifting the cholesterol linker handles from the shell-inner face to the shell-outer face of the triangle subunits. **b,** cryoEM micrographs of VCDs within their parent vesicle. Scale bars: 100 nm. **c,** Illustration of a bivesicular DNA shell (vesicle-coated DCV; VCDCV) contained in a parent vesicle, produced in a 2-step budding assay using triangles with orthogonal linker handles on their top and bottom faces. In the first step, the bottom face linkers are hybridised to cholesterol-modified DNA strands for DCV formation by outward budding. Then, DCVs are mixed with LVs carrying single-stranded linker handles complementary to those on the shell-outer face of the triangles, resulting in inward budding and VCDCV formation. As a result, VCDCVs have four layers: An inner vesicle stemming from the first step (orange), the DNA origami shell (white), an outer vesicle (pink) coupled to the shell by complementary linker handles, and the parent vesicle (purple) with its DNA linker handles (green blobs). **d,** cryoEM micrographs of VCDCVs. Images were Gaussian blurred and levelled for clarity. Scale bars: 100 nm.

363 # Materials and Methods

364 **Materials**

365 All chemicals were purchased from Sigma Aldrich and Carl Roth unless stated otherwise.
366 1,2-dioleoyl-sn-glycero-3-phosphocholine (DOPC) and 1,2-dioleoyl-sn-glycero-3-
367 phosphoethanolamine-N-(cap biotinyl) (biotinylated DOPE) were obtained from Avanti Polar
368 Lipids, and Atto488 and Atto643 modified 1,2-dioleoyl-sn-glycero-3-phosphoethanolamine
369 (DOPE) was obtained from Atto-Tec. NeutrAvidin was purchased from Thermo Scientific.
370 Regular DNA oligonucleotides were purchased from IDT, and modified oligonucleotides were
371 obtained from Biomers. Scaffold DNA was produced biotechnologically in-house.

372

373 **DNA origami folding, purification & quantification**

374 DNA origami triangles were folded as described previously[28]. Briefly, circular scaffold strands
375 of bacteriophage origin (p8064, 50 nM) and staple oligonucleotides (200 nM per staple) were
376 mixed in folding buffer (5 mM Tris base, 1 mM EDTA, 5 mM NaCl, pH 8) containing 20 mM
377 $MgCl_2$ and exposed to a thermal annealing ramp (65 °C, 15'; 58-53 °C, 1 h/°C; stored at 20 °C)
378 in a Tetrad2 (Bio-Rad) thermocycler. For some experiments, structures were fluorescently
379 labelled by including Atto643 labelled oligonucleotides in the folding reaction. The folded
380 product was purified by agarose gel electrophoresis by excising the leading band, crushing
381 the gel pieces and centrifuging them in 0.45 µm Costar Spin-X spin columns (Corning) for 10
382 min at 8 krcf. When needed, the purified structures were washed and concentrated by
383 ultrafiltration (Amicon Ultra 0.5 mL, 100 kDa cut-off, Millipore), exchanging the buffer for
384 folding buffer containing 5 mM $MgCl_2$ and 300 mM NaCl. Origami solutions were quantified
385 using a NanoDrop8000 spectrophotometer (Thermo Scientific).

386

387 **Vesicle preparation and quantification**

388 Giant vesicles were prepared by gentle swelling of dry lipid films on polyvinyl alcohol gels as
389 described previously[30], with slight modifications. A petri dish (⌀ 10 cm) was plasma cleaned
390 in a glow discharge device, and then 1800 µl of a 5% solution of polyvinyl alcohol (Mowiol
391 28-99, Sigma Aldrich) in ddH_2O was evenly distributed across its surface. The dish was
392 incubated for at least 30 min at 50 °C until a dry gel formed. Then, 162 µl of the lipid mixture
393 (DOPC with additional 0.5-1% fluorescently labelled DOPE (DOPE-Atto488 or DOPE-Atto643,
394 supplied by Atto-Tec) if visualisation by fluorescence was desired; 2.54 mM total lipid
395 concentration) in chloroform was evenly spread out across the surface using a Drigalski
396 spatula until the chloroform evaporated. Remaining traces of solvent were removed by

397 exposing the dried lipid cake to a vacuum for at least 15 min. Next, 4-5 mL of folding buffer
398 (+5 mM $MgCl_2$ and 300 mM NaCl) was added to the petri dish and the solution was left in a
399 humid chamber in the dark at RT for at least 1 h. GVs were detached by gently tapping against
400 the dish and pipetting up and down with a cut pipette tip. The GV suspension was stored at
401 4 °C in the dark.
402
403 When GVs were to be washed and concentrated, the dried lipid film was swollen in folding
404 buffer (+5 mM $MgCl_2$ and 320 mM CsCl) and, after harvesting, transferred into a falcon tube.
405 The tube was filled up with isosmotic buffer (folding buffer containing 5 mM $MgCl_2$ and 300
406 mM NaCl) and centrifuged for at least 30 min at 300 rcf. The supernatant was discarded, and
407 the GV pellet was washed 2-3 more times by adding 900 µl buffer and centrifuging the
408 suspension for 7 min at 300 rcf.
409
410 Smaller-sized vesicles were prepared using a mini-extruder (Avanti polar lipids) and
411 polycarbonate membranes with the desired pore size (400, 200, 50 nm; Whatman). GV
412 preparations were pushed back and forth through the membrane 21 times.
413
414 Lipids in vesicle preparations were quantified using a colourimetric phospholipid
415 quantification assay kit (Sigma Aldrich) following the manufacturer's instructions. The
416 absorbance was measured at 570 nm on a Clariostar plus microplate reader (BMG Labtech).
417 The result was extrapolated based on the molar composition of the lipid mix used to account
418 for PE species, which are not detectable by this method.
419
420 Buffer osmolalites were measured using an Osmomat 3000 freeze point osmometer
421 (Gonotec).
422
423 **Vesicle binding study**
424 Microscope slides and coverslips were washed with ddH_2O and incubated in denatured BSA
425 blocking buffer (10 mM TRIS, 150 mM NaCl, 50 µM BSA, pH 8) overnight as described
426 previously[33]. Next, the glassware was thoroughly washed with ddH_2O to remove residual
427 blocking buffer and dried at 50 °C for 1 h. 6 µl of GVs (99.95% DOPC, 0.05% DOPE-Atto488;
428 swollen in folding buffer (+5 mM $MgCl_2$, 280 mM sucrose) was mixed with origami triangles
429 (+/- cholesterol modified strands; fluorescently labelled with Atto643 modified
430 oligonucleotides; final origami concentration: 7 nM) and topped up to 40 µl with folding buffer
431 (+5 mM $MgCl_2$, 280 mM glucose). 300 mM NaCl was added to samples testing the effect of

432 elevated sodium on the binding behaviour of origami. The samples were pipetted into an
433 imaging chamber formed by sandwiching a silicon isolator (Grace Bio-Labs) between
434 passivated coverslips and microscope slides. The samples were imaged using a Leica TCS
435 SP5 confocal microscope with a Leica HCX PL APO CS 63x/1.40-0.60 oil immersion
436 objective.
437
438 **Budding assays**
439 Vesicles were prepared as described above using 99.0 – 100% DOPC with the remainder
440 being fluorescently labelled DOPE if visualisation by fluorescence was desired. Origami
441 triangles were hybridised to cholesterol-modified oligonucleotides by adding them at a 1.5 x
442 excess with respect to the total amount of compatible linker handles on the origami. The
443 hybridisation reaction was incubated at RT for at least 30 min. For outward budding reactions,
444 24 µl of untreated GV suspension was mixed with origami triangles with linker handles on the
445 shell-inward face at a final concentration of approx. 2 nM origami. In experiments where lipid
446 quantities in GV preparations were known, 1000 pmol lipid of the GV suspension was mixed
447 with the origami (6 µl at 10 nM). The sample was topped up to 30 µl with folding buffer (+5
448 mM $MgCl_2$, 300 mM NaCl), and the $MgCl_2$ concentration was adjusted to 65 mM by adding
449 1 M $MgCl_2$ solution (hyperosmotic conditions) or to 60 mM by adding folding buffer (+210
450 mM $MgCl_2$; isosmotic conditions). Budding reactions were incubated at 37 °C for 1-3 d.
451
452 For inward budding reactions, samples were prepared in the same way with the difference
453 that origami triangles (3 µl at 20 nM) with linker handles on the shell-outward face were mixed
454 with LVs (1500 pmol lipids; approx. 200 nm diameter).
455
456 For bivesicular DNA shells (VCDCVs), triangles with orthogonal linker handles on the top and
457 bottom face were used, and inward and outward budding reactions were conducted
458 successively. First, DCVs were produced in an outward budding assay (1200 µl in total) using
459 cholesterol-modified oligonucleotides hybridised to the bottom face linker handles. The
460 sample was then centrifuged at 300 rcf for 5-8 min, and the pellet containing residual GVs
461 was discarded. The supernatant was then ultracentrifuged at 55 krpm (avg. 108 krcf) for 30
462 min in a Beckman Coulter Optima MAX-TL ultracentrifuge equipped with a TLA-110 fixed
463 angle rotor. 80-90% of the supernatant was removed, and the pellet was resuspended in the
464 remaining volume.
465 Meanwhile, LVs (200 nm diameter) were mixed with a second cholesterol-bearing
466 oligonucleotide complementary to the linker handles on the top face of the triangles. These

467 oligonucleotides were added at a 50x excess with respect to the total amount of
468 complementary linker handles on the origami, and the solution was incubated at RT for 15-
469 30 min. Then, the magnesium concentration in the LV solution was adjusted to 60 mM $MgCl_2$
470 by adding an isosmotic folding buffer containing 210 mM $MgCl_2$. Finally, LVs (1500 pmol
471 lipids) were mixed with the DCV concentrate (to a final concentration of 1-5 nM DNA), and
472 the samples were incubated at 37 °C for 1-3 d.
473
474 **Budding using biotin-NeutrAvidin**
475 For budding reactions using biotin-NeutrAvidin interactions to anchor triangles to the
476 membranes, GVs containing 3% biotinylated DOPE, 1% fluorescently labelled DOPE and 96%
477 DOPC were prepared. Origami triangles were folded with linker handles for biotinylated
478 oligonucleotides and linker handles for purification using magnetic beads. Biotinylated
479 oligonucleotides were already included in the folding reaction to remove unbound strands
480 and excess staples by gel extraction. The triangles were then mixed with a 500-fold excess
481 of NeutrAvidin and incubated for 1 h at 37 °C on an orbital shaker. Next, the sample was
482 transferred into a tube previously passivated with denatured BSA blocking buffer and mixed
483 with magnetic beads (Dynabeads M-270 Streptavidin, Invitrogen) coated with DNA strands
484 complementary to a section of the purification linker handles on the triangles. The sample
485 was incubated for 1 h at RT on a rotary shaker, and the beads now carrying the origami
486 triangles were washed 3-4 times with folding buffer containing 5 mM $MgCl_2$ and 300 mM
487 NaCl. Finally, an invader strand complementary to the full length of the purification linker
488 handles was added in great excess, and the solution was incubated at 37 °C for 1 h to
489 uncouple the origami from the magnetic beads by strand displacement. The NeutrAvidin
490 bearing triangles were then mixed with biotinylated GVs, and the $MgCl_2$ concentration was
491 adjusted to 65 mM by adding 1 M $MgCl_2$ solution (hyperosmotic conditions) or to 60 mM by
492 adding folding buffer (+210 mM $MgCl_2$; isosmotic conditions). The sample was incubated at
493 37 °C for 2.5 d.
494
495 **Negative-staining transmission electron microscopy**
496 Sample solutions were incubated on glow-discharged copper grids (400 mesh) with a carbon
497 support film (Science Services) for 4-8 minutes, depending on the sample concentration. The
498 solution was then blotted off using filter paper (Whatman). Then, the grid was washed once
499 using stain solution (2% aqueous uranyl formate + 25 mM NaOH), followed by incubating
500 another stain droplet on the grid for 30 s. Excess stain was blotted off using filter paper, and
501 the grid was air-dried before imaging.

502

503 Grids were typically imaged at x26-30k magnification using SerialEM with an FEI Tecnai T12
504 electron microscope operated at 120kV and a Tietz TEMCAM-F416 camera. Image contrast
505 was auto-levelled using Fiji[34].
506 For tomography, one-directional tilt series were acquired from -50° to +50° in steps of 2°
507 using SerialEM. The resulting image stacks were imported into Etomo (IMOD[35]), and images
508 were aligned without fiducials by cross-correlation with cumulative correlation switched on.
509 Tomograms were generated by filtered back-projection (gaussian filter cut-off: 0.35; fall-off:
510 0.035;). For visualisation, the z-stacks thus generated were imported into Fiji and z-projected
511 by summing up z-slices corresponding to the top, middle and bottom sections of the
512 respective particle of interest.

513 **Cryogenic electron microscopy**

514 Sample grids for cryoEM were prepared using an automated vitrification system (FEI Vitrobot
515 Mark V). First, grids (Quantifoil R1.2/1.3, Cu 200 mesh, 100 holey carbon films, 2 nm carbon
516 support film; for images of DCVs: Ted Pella, Cu 400 mesh, lacey carbon, <3 nm carbon
517 support film) were glow-discharged and then inserted into the Vitrobot. The conditions inside
518 the device's environmental chamber were kept at either 4 °C or 22 °C and 100% relative
519 humidity. Samples were typically incubated on the grids inside the chamber for 5 min and
520 plunge-frozen in liquid ethane (blot force: -1, 0 or 25; blot time: 2-3 s; blot total: 1; drain time:
521 0 s;). The grids were imaged with a spherical-aberration (Cs)-corrected Titan Krios G2
522 electron microscope (Thermo Fisher) operated at 300kV and equipped with a Falcon III 4k
523 direct electron detector (Thermo Fisher). Samples were imaged at x29k magnification and
524 defocus values between -1 and -4 µm. Images were auto-levelled in Fiji.
525

526 **Agarose gel electrophoresis and gel quantification**

527 Agarose gels were cast by dissolving UltraPure agarose (Invitrogen) in running buffer (0.5 x
528 TBE, Carl Roth) supplemented with $MgCl_2$ and optionally ethidium bromide (0.025%, Carl
529 Roth). Samples were run for 2 h at 90 V and then scanned using a Typhoon FLA 9500 laser
530 scanner (GE Healthcare) at a pixel size of 50 µm. Gels containing only monomeric origami
531 structures were run with 5.5 mM $MgCl_2$ in the gel and running buffer and an agarose
532 concentration of 1.5%. To resolve and preserve assembled shell structures, the gel and
533 running buffer were supplemented with 20 mM $MgCl_2$ and the agarose concentration was
534 reduced to 0.8%. Due to the elevated salt concentration in these gels, the gel boxes were
535 cooled in a water-ice bath, and the running buffer was exchanged every 45 min to replenish

lost magnesium. For visualisation, aggregates in the pockets were oversaturated, and the bands' contrast underneath was auto-levelled.

Gel lanes were quantified using Fiji. Images were processed by removing outliers (radius: 5.0 pixels; pixel threshold: 200;), spanning a rectangular selection box across the region of interest and plotting its intensity profile. Peak valleys were connected by straight lines, and the area between the peaks and the added lines was measured. The resulting values were normalised against the largest value in the same gel.

References

1. Votteler, J. & Sundquist, W. I. Virus Budding and the ESCRT Pathway. *Cell Host Microbe* **14**, 232–241 (2013).
2. Kaksonen, M. & Roux, A. Mechanisms of clathrin-mediated endocytosis. *Nat. Rev. Mol. Cell Biol.* **19**, 313–326 (2018).
3. Crowther, R. A., Pinch, J. T. & Pearse, B. M. F. On the structure of coated vesicles. *J. Mol. Biol.* **103**, 785–798 (1976).
4. Morris, K. L. *et al.* Cryo-EM of multiple cage architectures reveals a universal mode of clathrin self-assembly. *Nat. Struct. Mol. Biol.* **26**, 890–898 (2019).
5. Rothemund, P. W. K. Folding DNA to create nanoscale shapes and patterns. *Nature* **440**, 297–302 (2006).
6. Douglas, S. M. *et al.* Self-assembly of DNA into nanoscale three-dimensional shapes. *Nature* **459**, 414–418 (2009).
7. Dey, S. *et al.* DNA origami. *Nat. Rev. Methods Primer* **1**, 1–24 (2021).
8. Wagenbauer, K. F., Sigl, C. & Dietz, H. Gigadalton-scale shape-programmable DNA assemblies. *Nature* **552**, 78–83 (2017).
9. Wintersinger, C. M. *et al.* Multi-micron crisscross structures grown from DNA-origami slats. *Nat. Nanotechnol.* **18**, 281–289 (2023).
10. Ong, L. L. *et al.* Programmable self-assembly of three-dimensional nanostructures from 10,000 unique components. *Nature* **552**, 72–77 (2017).
11. Tikhomirov, G., Petersen, P. & Qian, L. Fractal assembly of micrometre-scale DNA origami arrays with arbitrary patterns. *Nature* **552**, 67–71 (2017).
12. Langecker, M. *et al.* Synthetic Lipid Membrane Channels Formed by Designed DNA Nanostructures. *Science* **338**, 932–936 (2012).
13. Burns, J. R., Stulz, E. & Howorka, S. Self-Assembled DNA Nanopores That Span Lipid Bilayers. *Nano Lett.* **13**, 2351–2356 (2013).
14. Burns, J. R. *et al.* Lipid-Bilayer-Spanning DNA Nanopores with a Bifunctional Porphyrin Anchor. *Angew. Chem. Int. Ed.* **52**, 12069–12072 (2013).
15. Khmelinskaia, A., Mücksch, J., Petrov, E. P., Franquelim, H. G. & Schwille, P. Control of Membrane Binding and Diffusion of Cholesteryl-Modified DNA Origami Nanostructures by DNA Spacers. *Langmuir* **34**, 14921–14931 (2018).
16. Journot, C. M. A., Ramakrishna, V., Wallace, M. I. & Turberfield, A. J. Modifying Membrane Morphology and Interactions with DNA Origami Clathrin-Mimic Networks. *ACS Nano* **13**, 9973–9979 (2019).

579 17. Grome, M. W., Zhang, Z., Pincet, F. & Lin, C. Vesicle Tubulation with Self-Assembling
580 DNA Nanosprings. *Angew. Chem. Int. Ed.* **57**, 5330–5334 (2018).
581 18. Liu, L., Xiong, Q., Xie, C., Pincet, F. & Lin, C. Actuating tension-loaded DNA clamps
582 drives membrane tubulation. *Sci. Adv.* **8**, eadd1830 (2022).
583 19. Franquelim, H. G., Khmelinskaia, A., Sobczak, J.-P., Dietz, H. & Schwille, P.
584 Membrane sculpting by curved DNA origami scaffolds. *Nat. Commun.* **9**, 811 (2018).
585 20. Yang, J. *et al.* Modulating Lipid Membrane Morphology by Dynamic DNA Origami
586 Networks. *Nano Lett.* **23**, 6330–6336 (2023).
587 21. Baumann, K. N. *et al.* Coating and Stabilization of Liposomes by Clathrin-Inspired
588 DNA Self-Assembly. *ACS Nano* **14**, 2316–2323 (2020).
589 22. Kocabey, S. *et al.* Membrane-Assisted Growth of DNA Origami Nanostructure Arrays.
590 *ACS Nano* **9**, 3530–3539 (2015).
591 23. Bassereau, P., Sorre, B. & Lévy, A. Bending lipid membranes: Experiments after W.
592 Helfrich's model. *Adv. Colloid Interface Sci.* **208**, 47–57 (2014).
593 24. Simunovic, M., Evergren, E., Callan-Jones, A. & Bassereau, P. Curving Cells Inside
594 and Out: Roles of BAR Domain Proteins in Membrane Shaping and Its Cellular Implications.
595 *Annu. Rev. Cell Dev. Biol.* **35**, 111–129 (2019).
596 25. Sweitzer, S. M. & Hinshaw, J. E. Dynamin Undergoes a GTP-Dependent
597 Conformational Change Causing Vesiculation. *Cell* **93**, 1021–1029 (1998).
598 26. Boucrot, E. *et al.* Membrane Fission Is Promoted by Insertion of Amphipathic Helices
599 and Is Restricted by Crescent BAR Domains. *Cell* **149**, 124–136 (2012).
600 27. Rossman, J. S., Jing, X., Leser, G. P. & Lamb, R. A. Influenza Virus M2 Protein
601 Mediates ESCRT-Independent Membrane Scission. *Cell* **142**, 902–913 (2010).
602 28. Sigl, C. *et al.* Programmable icosahedral shell system for virus trapping. *Nat. Mater.*
603 **20**, 1281–1289 (2021).
604 29. Gerling, T., Wagenbauer, K. F., Neuner, A. M. & Dietz, H. Dynamic DNA devices and
605 assemblies formed by shape-complementary, non–base pairing 3D components. *Science*
606 **347**, 1446–1452 (2015).
607 30. Weinberger, A. *et al.* Gel-Assisted Formation of Giant Unilamellar Vesicles. *Biophys.*
608 *J.* **105**, 154–164 (2013).
609 31. Dannhauser, P. N. & Ungewickell, E. J. Reconstitution of clathrin-coated bud and
610 vesicle formation with minimal components. *Nat. Cell Biol.* **14**, 634–639 (2012).
611 32. Ford, M. G. J. *et al.* Curvature of clathrin-coated pits driven by epsin. *Nature* **419**,
612 361–366 (2002).

33. Park, J. H. *et al.* Temperature-Induced Denaturation of BSA Protein Molecules for Improved Surface Passivation Coatings. *ACS Appl. Mater. Interfaces* **10**, 32047–32057 (2018).

34. Schindelin, J. *et al.* Fiji: an open-source platform for biological-image analysis. *Nat. Methods* **9**, 676–682 (2012).

35. Kremer, J. R., Mastronarde, D. N. & McIntosh, J. R. Computer Visualization of Three-Dimensional Image Data Using IMOD. *J. Struct. Biol.* **116**, 71–76 (1996).

SUPPLEMENTARY INFORMATION

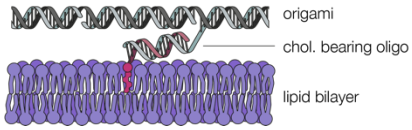

Supplementary Figure 1 | Attachment of origami triangles to vesicles via cholesterol-bearing oligonucleotides. Linker handles extending from the origami surface are hybridised to cholesterol-bearing oligonucleotides with complementary sequences. Cholesterol acts as a lipid membrane anchor to tether the triangles to lipid vesicles.

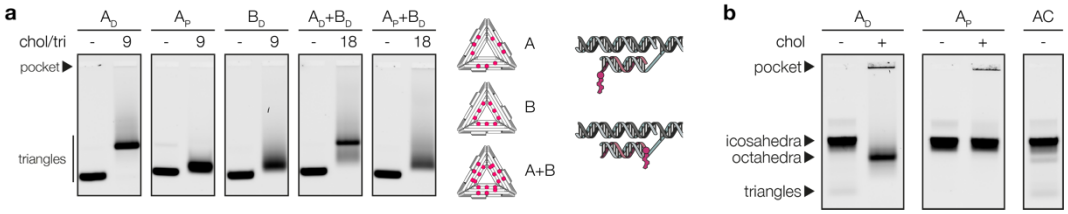

Supplementary Figure 2 | The influence of cholesterol position and orientation on origami triangles. (**a**) The overall reach of cholesterol-bearing oligonucleotides (chol-oligo) determines the migration behaviour of origami triangles. When cholesterols are positioned closer to the outer edge and the stacking contacts in a distal configuration (A_D), bands in an agarose gel appear shifted and smeared compared to the same triangles not hybridised to chol-oligos. This effect could be reduced by changing the orientation of the cholesterol to a proximal configuration with respect to the origami, such that the reach of the cholesterol is minimised (A_P). When chol-oligos are positioned closer to the centre of the structure, and thus further away from the stacking contacts, the migration distance of these triangles is comparable to that of sample A_P, albeit with more smearing. Combining both variants to double the cholesterol count per triangle from 9 to 18 moieties yielded bands appearing as combinations of the individual variants. (**b**) The reach of cholesterol influences the assembly of cholesterol-decorated triangles. An assembly control (AC) of triangles lacking protruding linker handles assembles mostly into icosahedral species, as do triangles with protruding linker handles not hybridised to chol-oligos. When chol-oligos are introduced, distal cholesterol (A_D) promotes the formation of primarily octahedral species, whereas proximal cholesterol (A_P) does not noticeably influence the assembly behaviour. Reducing the reach of

individual cholesterols either by positioning them closer to the centre of the triangles or by choosing proximal configurations reduces unwanted interactions.

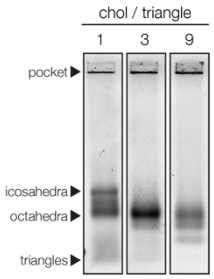

Supplementary Figure 3 | The influence of cholesterols per triangle in assembly reaction containing GVs. Whilst optimising cholesterol positioning on the triangle can reduce unexpected assembly behaviour, introducing lipid vesicles yet again shifts the assembly towards octahedra, the degree of which increases with the number of cholesterols per triangle.

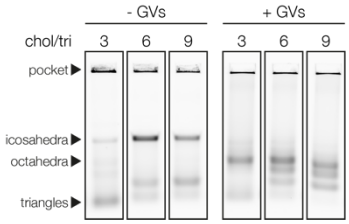

Supplementary Figure 4 | GVs shift the assembly of cholesterol-bearing triangles towards octahedral shells. The assembly behaviour of cholesterol-bearing triangles, tagged with Atto643 for visualisation, depends on the presence or absence of GVs. Without GVs, triangles mainly assemble into icosahedral shells as per their design. With GVs, however, most shells detected by agarose gel electrophoresis are octahedral. The abundance of smaller, intermediate species between closed shells and monomeric triangles increases with the number of cholesterols per triangle and mostly represents aggregated triangles.

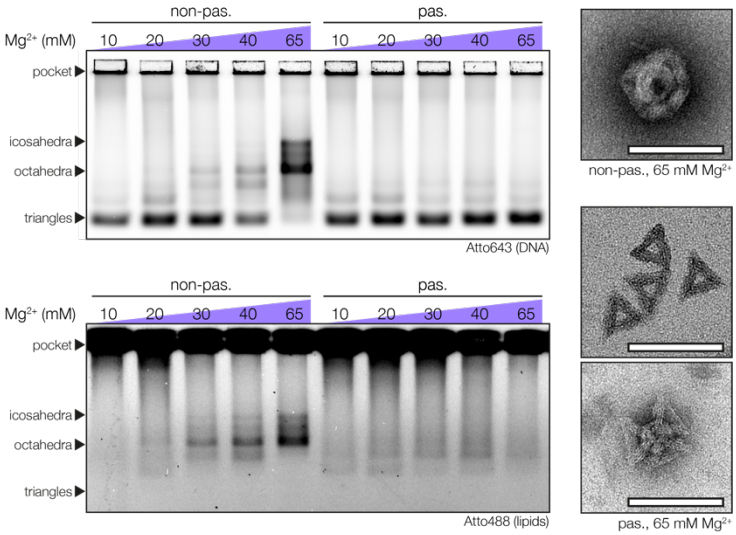

Supplementary Figure 5 | Triangle assembly is the driving force behind DCV formation. The importance of shell assembly for DCV formation was studied by incubating triangles at various $MgCl_2$ concentrations at (65 mM) or below (10-40 mM) the typical threshold concentration for shell assembly. For visualisation by agarose gel electrophoresis, the triangles were hybridised to Atto643 bearing oligonucleotides, and the GVs contained a fraction of Atto488 labelled DOPE. Furthermore, two triangle species were prepared: A non-passivated version with blunt-ended stacking contacts and a passivated version where the staple oligonucleotides at the base stacking contacts were extended by introducing additional unpaired thymidines. Whereas the non-passivated version formed DCVs as seen by the bands in the lipid channel (lower panel) colocalising with the shells in the DNA channel (upper panel), only faint bands below the typical height of DNA shells were found in samples containing the passivated version. These results were compared by TEM, which further revealed that while the passivated triangle samples contained mostly monomeric triangles, there was a small number of aggregated triangles held together by small vesicles, likely representing the faint bands. Shell assembly is, therefore, a main factor behind DCV formation. Scale bars: 100 nm.

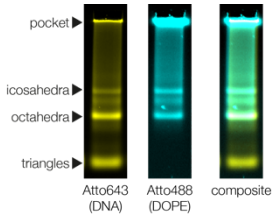

692
693
694 **Supplementary Figure 6 | Analysis of DCV formation by colocalisation analysis of DNA**
695 **and lipid bands.** The relative efficiency of DCV formation could be analysed by agarose gel
696 electrophoresis using fluorescently labelled DNA oligos attached to the origami structure or
697 ethidium bromide, and a small fraction of fluorescently labelled DOPE species in the lipid
698 mixture comprising the vesicles. Whereas multiple bands were detected in the DNA channel
699 representing triangles in monomeric or assembled states, lipid signal was only seen at the
700 height of assembled shells. The absence of lipid signal colocalised with monomeric triangles
701 suggests that lipids predominantly enter the gel as part of a DCV. The gel pockets contain
702 origami-coated GVs, which were oversaturated to better visualise the much fainter bands
703 below.
704

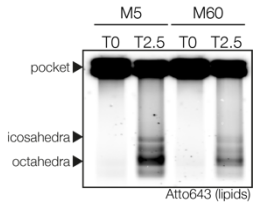

705
706
707 **Supplementary Figure 7 | Shell preassembly reduces DCV yields.** Cholesterol-bearing
708 origami triangles were incubated without GVs (containing a small fraction of DOPE-Atto643)
709 for 4 h at 37 °C in either 5 mM (monomer conditions) or 60 mM (assembly conditions) $MgCl_2$
710 to study the effect partially assembled shells have on DCV yields. Afterwards, GVs were
711 added, and the $MgCl_2$ concentration in the 5 mM controls was increased to 60 mM. Aliquots
712 taken and frozen at t = 0 d were compared to samples incubated at 37 °C for 2.5 d using
713 agarose gel electrophoresis, and DCV yields were analysed by comparing lipid bands.
714 Whereas t = 0 d aliquots looked alike in samples pre-incubated in either 5 mM or 60 mM
715 $MgCl_2$, we finally obtained stronger lipid signals in samples initially incubated at 5 mM. We
716 deduce that DCVs form best when monomeric triangles are assembled directly on the
717 membrane. Partially assembled shells may fail to bind GVs efficiently due to steric hindrance,
718 resulting in reduced DCV yields.
719